# Steady-state kinetics of the autocatalytic zymogen activation: A comparison with the Michaelis–Menten reaction mechanism

Malgorzata Anna Tyczynska[1], Justin Eilertsen[1], and Santiago Schnell[1,2,3]

[1]*Department of Molecular & Integrative Physiology, University of Michigan Medical School, Ann Arbor, Michigan, USA*
[2]*Department of Computational Medicine & Bioinformatics, University of Michigan Medical School, Ann Arbor, Michigan, USA*
[3]*E-mail: schnells@umich.edu*

**Abstract**

A zymogen is an inactive precursor of an enzyme, which needs to go through a chemical change to become an active enzyme. The general intermolecular mechanism for the autocatalytic activation of zymogens is governed by the single-enzyme, single-substrate catalyzed reaction following the Michaelis–Menten mechanism of enzyme action, where the substrate is the zymogen and product is the same enzyme catalyzing the reaction. In this article we investigate the nonlinear chemical dynamics of the intermolecular autocatalytic zymogen activation reaction mechanism, and compare it to that of the Michaelis–Menten reaction mechanism. We show that the intermolecular autocatalytic zymogen activation exhibits significant changes in reaction dynamics relative to the Michaelis–Menten reaction mechanism. These changes include differences in the number of conservation laws, number and stability of equilibrium states, altered structure of the invariant set that influences the long-time rate of the reaction, and qualitative evolution of the reaction depending strictly on the choice of initial conditions. We find a rate law, homologous to the Michaelis–Menten equation, to estimate the kinetic parameters of the intermolecular autocatalytic zymogen activation reaction mechanism, and derive the conditions for the validity for this rate law. Finally, we derive analytical expressions to estimate the timescale for the completion of the zymogen activation, which could have a practical application to calculate the molar enthalpy $\Delta H_{app}$ of the autocatalytic zymogen reaction in calorimetry assays.

# 1 Introduction

Steady-state systems provide a simple means of measuring the kinetic parameters of an enzyme catalyzed reaction. Perhaps the most widely recognized steady-state kinetics rate law is the Michaelis–Menten (MM) equation:

$$\frac{\mathrm{d}p}{\mathrm{d}t} = -\frac{\mathrm{d}s}{\mathrm{d}t} \simeq \frac{v\,s}{K_M + s}, \tag{1}$$

where $p$ denotes the product concentration over time, $s$ denotes substrate concentration over time, $v$ is the limiting rate and $K_M$ is the Michaelis constant [1, 2]. Equation (1) is typically derived by applying a mathematical model reduction technique – known as the quasi-steady-state approximation (QSSA) – to the MM reaction mechanism [3]

$$S + E \underset{k_{-1}}{\overset{k_1}{\rightleftharpoons}} C \xrightarrow{k_2} E + P. \tag{2}$$

In reaction scheme (2), the enzyme, $E$, binds to the substrate, $S$, and forms an intermediate complex, $C$. The complex then dissociates into either an enzyme molecule and a product, $P$, or to the original reactants. The constants $k_1$, $k_{-1}$ and $k_2$ denote reaction rates.

The MM equation (1) can be used to estimate $v$ and $K_M$ as long as specific reaction conditions are met [3, 4]. Since the 1950s, steady-state kinetics has been extensively used to estimate kinetic parameters through progress curve or initial rate experiments [5, 6]. The popularity of the MM equation (1) has substantially grown since the beginning of the century due to the implementation of systems biology approaches to model biochemical processes [7]. Nevertheless, despite the undeniable significance of the steady-state kinetics, one question remains unanswered for enzyme catalyzed reactions: do the properties of MM steady-state kinetics prevail for autocatalytic enzyme catalyzed reactions?

Zymogens are enzyme precursors (proenzymes) that can be activated through non-catalytic [8] or catalytic reactions, and have numerous biochemical functions. For example, they play a critical role in protein digestion by converting pepsin to pepsinogen [8, 9], and trypsin to trypsinogen [10, 11, 12]. Activation can occur in three ways: (i) The inactive enzyme can be activated by another enzyme that cleaves off a peptide unit; this is the mechanism we consider in this work. (ii) The configuration of the zymogen can be changed in order to reveal the activation site. (iii) The inactive substance is activated when a coenzyme binds to the zymogen. A simple autocatalytic reaction that utilizes mechanism (i) is the activation of trypsinogen by trypsin [13, 14], while the activation of pepsinogen to active pepsin at low pH [5] follows mechanism (ii).

Mechanism (i) is represented schematically by

$$S + E \underset{k_{-1}}{\overset{k_1}{\rightleftharpoons}} C \xrightarrow{k_2} 2E + W, \tag{3}$$

where $S$ is a zymogen, $E$ is an active enzyme, $W$ is peptide, and $k_1, k_2$ and $k_{-1}$ are rate constants. We refer to (3) as the intermolecular autocatalytic zymogen activation (IAZA) reaction. In addition, Fuentes [15] proposed a mechanism for zymogen activation that consists of two reaction pathways. One pathway consists of an intramolecular non-catalytic step in which the zymogen molecule disassociates into an active enzyme and a peptide

$$S \xrightarrow{k_d} E + W, \tag{4}$$

while the additional catalytic step in the second pathway follows the IAZA reaction mechanism (3). More complicated models of zymogen activation have been analyzed in the context of a coupled enzyme assay that consists of an *indicator* reaction [16]. The model analyzed in [16] can be used to describe the activation of protein C by thrombin. However, neither reaction studied in [16] is autocatalytic, and thus a proper nonlinear analysis of a basic autocatalytic process through which zymogens are activated is currently lacking. This paper serves as a preliminary first step towards understanding such autocatalytic enzyme reaction mechanisms.

The significance of the IAZA reaction has motivated enzymologists to derive rate equations that describe the progress curves for zymogen activation [13], the steady-state or rapid equilibrium kinetic of zymogen action in the presence of reversible inhibitors [17], competitive and noncompetitive inhibitors [18], as well as complex inter- and intramolecular zymogen activation [15, 19, 20]. Although rate equations are derived

under the presupposition of steady-state kinetics or QSSA, in many of studies of zymogen activation the steady-state kinetics assumption (or QSSA) has not been properly motivated through the traditional method of scaling [21, 22], or through more modern methods that have recently been developed [23, 24, 25, 26].

In the sections that follow, we investigate the nonlinear dynamics of the IAZA reaction mechanism (3) by comparing its behavior with the well characterized dynamics of the MM reaction mechanism (2). This is accomplished in consecutive steps. First, the phase–plane geometry of the IAZA reaction mechanism is inspected and compared to the MM reaction mechanism. Then, the dynamics of both reaction mechanisms are numerically simulated and analyzed via scaling arguments. We derive a quasi-steady-state (QSS) rate law that can be utilized to estimate the relevant kinetic parameters of the IAZA reaction mechanism through initial rate experiments. We also derive the conditions for the validity of QSSA, and discuss its range of applicability in experiments. Finally, we estimate the timescale for the completion of the zymogen activation that is valid when the QSSA holds; this has practical implications for calorimetry enzyme assays experimental design and interpretation. The results reported in this work can be applied to other zymogen reaction mechanisms studied by Fuentes, García-Moreno, Valero, Varón and co-workers, such as the two-pathway mechanism in [15].

## 2 The intermolecular autocatalytic zymogen activation reaction mechanism

In this section, we apply the law of mass action to (3), which admits a mathematical model that describes the temporal dynamics of the IAZA reaction. This model permits us to investigate, as well as compare and contrast, the nonlinear dynamics and phase–plane geometries of the IAZA reaction mechanism (3) with the MM reaction mechanism (2). For the specific analysis of MM reaction mechanism (2), we refer the reader to references [27, 28, 29].

Let $s := s(t)$, $e := e(t)$ and $c := c(t)$ denote the concentrations of $S$, $E$, and $C$ respectively. Applying the law of mass action yields:

$$\frac{\mathrm{d}s}{\mathrm{d}t} = -k_1 es + k_{-1} c, \tag{5a}$$

$$\frac{\mathrm{d}c}{\mathrm{d}t} = k_1 es - (k_{-1} + k_2) c, \tag{5b}$$

$$\frac{\mathrm{d}e}{\mathrm{d}t} = -k_1 es + (k_{-1} + 2k_2) c, \tag{5c}$$

$$\frac{\mathrm{d}w}{\mathrm{d}t} = k_2 c. \tag{5d}$$

Note that equations (5a)–(5c) admit a conservation law:

$$\frac{\mathrm{d}s}{\mathrm{d}t} + \frac{\mathrm{d}e}{\mathrm{d}t} + 2\frac{\mathrm{d}c}{\mathrm{d}t} = 0. \tag{6}$$

Typically, experimental initial conditions are given by

$$s(0) = s_0, \qquad e(0) = e_0, \qquad c(0) = 0, \tag{7}$$

and we will assume (7) holds in the analysis that follows. As we shall discuss later, the typical behavior of the IAZA system (5a)–(5d) depends on the relation between $s_0$ and $e_0$; this is illustrated on FIGURE 1.

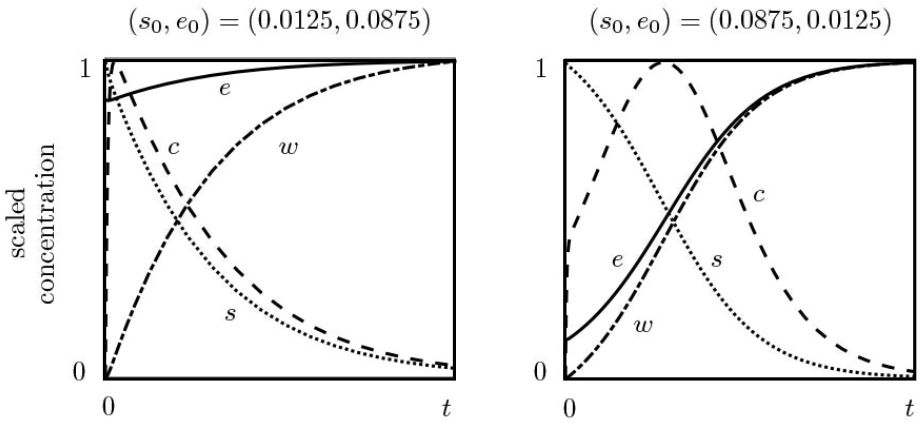


Figure 1: **The relation between $s_0$ and $e_0$ influences the behavior of the IAZA time course trajectories** (5a)–(5d)**.** Each panel illustrates the $s$, $e$, $c$ and $w$ normalized with respect to their maximum value. Initial concentrations for $s$ and $e$ are given at the top of each figure panel and $w_0 = c_0 = 0$ as assumed by (7). The initial conditions and parameter values are in arbitrary units for illustrative purposes, and the rate constants are of the same order of magnitude ($k_1 = k_2 = k_{-1} = 1$).

Combining (6) with (7) yields $s + e + 2c = E_T$, where $E_T$ is the total concentration of zymogen and enzyme; $E_T = s_0 + e_0$. Substituting $e = E_T - s - c$ into (5a)–(5b) yields

$$\frac{\mathrm{d}s}{\mathrm{d}t} = k_1\Big[ -(E_T - s)s + (K_S + 2s)c\Big], \tag{8a}$$

$$\frac{\mathrm{d}c}{\mathrm{d}t} = k_1\Big[(E_T - s)s - (K_M + 2s)c\Big], \tag{8b}$$

where $K_S = k_{-1}/k_1$ is the equilibrium constant of the intermediate complex, $K = k_2/k_1$ is the Van Slyke–Cullen and $K_M = K_S + K$ denote the Michaelis constant of the IAZA reaction respectively. For simplicity, $W$ has been ignored since it is mathematically recoverable from $s$ and $c$. The constant $E_T$ is the unique conserved quantity that arises from (6)

$$E_T = e + s + 2c. \tag{9}$$

From the biochemical point of view, the initial conditions (7) define the constant $E_T$ as the sum of initial reactant concentrations $E_T = e_0 + s_0$; this implies that $e = E_T$ upon completion of the reaction and imposes an upper bound on the initial concentration of zymogen: $0 \leq s_0 \leq E_T$. Note that the presence of just one conservation law (9) in the IAZA reaction mechanism (3) is in contrast to the MM reaction (2), which has two independent conservation laws: one for the enzyme ($e + c = e_0$), and another for the substrate ($s + c + p = s_0$).

## 2.1 The geometrical picture of intermolecular autocatalytic zymogen activation reaction mechanism

The governing equations of the IAZA reaction mechanism (8a)–(8b) are nonlinear, and exhibit two equilibrium points:

$$x_1^* = (0, 0) \quad \text{and} \quad x_2^* = (E_T, 0). \tag{10}$$

The stability of equilibrium points (10) is conventionally determined by analyzing the Jacobian of the system (8a)–(8b) near these points. We find that $x_1^*$ is a stable point and $x_2^*$ is a saddle point. Since $x_2^*$ is a saddle point, it has one-dimensional stable $\mathcal{W}^s$ and unstable $\mathcal{W}^u$ manifolds. As we illustrate in FIGURE 2, the presence of $\mathcal{W}^u$ plays a critical role in uncovering the $c$–$s$ phase–plane geometry: $\mathcal{W}^u$ connects $x_1^*$ and $x_2^*$ and forms a heteroclinic orbit, $\Gamma_{\mathcal{W}}$, which is an invariant manifold that can potentially influence the long-time dynamics of the IAZA reaction. The existence of $\Gamma_{\mathcal{W}}$ is verified numerically using MATCONT

open source software [30] (see [31] for details about the numerical algorithm utilized to track $\Gamma_{\mathcal{W}}$). Note, that the presence of $\Gamma_{\mathcal{W}}$ contrasts the geometry of MM reaction kinetics, which consist of a stable equilibrium at origin and a slow, invariant manifold [28].

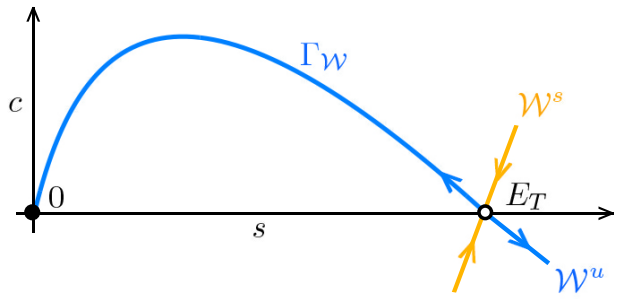


Figure 2: **The geometry of the IAZA reaction mechanism** (3) **is characterized by the presence of heteroclinic orbit $\Gamma_{\mathcal{W}}$.** The system (8a)–(8b) has a stable equilibrium $x_1^* = (0, 0)$ (the solid black circle) and the saddle equilibrium $x_2^* = (E_T, 0)$ (open circle). The heteroclinic orbit $\Gamma_{\mathcal{W}}$ that connects $x_1^*$ and $x_2^*$ is the solid blue curve, and the stable manifold corresponding to $x_2^*$ is the solid yellow curve.

Following [28], the shape of $\Gamma_{\mathcal{W}}$ in the $c$–$s$ phase–plane is interpreted relative to the $c$-nullcline, $\mathcal{N}_c(s)$, and the $s$-nullcline, $\mathcal{N}_s(s)$:

$$\mathcal{N}_c(s) = \frac{(E_T - s)s}{K_M + 2s}, \qquad \mathcal{N}_s(s) = \frac{(E_T - s)s}{K_M - K + 2s}. \tag{11}$$

The $c$-nullcline corresponds to the zeroth-order approximation to the QSS dynamics of (8a)–(8b), and the $s$-nullcline corresponds to the zeroth-order approximation to rapid equilibrium of (8a)–(8b). In the $c$–$s$ phase–plane, both nullclines, as well as $\Gamma_{\mathcal{W}}$, intersect at the equilibria (10). Due to the form of (11), the $c$- and $s$-nullclines are characterized by unimodal curves on the interval $[0, E_T]$, and with a maximum present at $s$ equal to $s_c^*$ and $s_s^*$ respectively. It is easy to verify that:

$$s_c^* \simeq s_s^* \simeq \frac{E_T}{2} \text{ when } K_M \gg E_T. \tag{12}$$

The above condition for the equality of maxima can be written as

$$\varepsilon \equiv \frac{E_T}{K_M} \ll 1, \tag{13}$$

but we note that the approximation of $s_c^*$ is valid whenever $E_T \ll K_S$, which is less restrictive than (12). When (13) is satisfied, the nullclines assume their maximum values near $s = E_T/2$, as shown in FIGURE 2. Furthermore, FIGURE 2 also reveals the nature of $\Gamma_{\mathcal{W}}$: it remains under $\mathcal{N}_c$ for $s_c^* < s < E_T$, crosses it at $s \approx s_c^*$, and approaches the origin while staying between $\mathcal{N}_c$ and $\mathcal{N}_s$. The value of $s$ at which $\mathcal{N}_s$ and $\Gamma_{\mathcal{W}}$ intersect is only approximately $s_c^*$, since $\Gamma_{\mathcal{W}}$ has been tracked numerically using MATCONT [30]. Nevertheless, the precision of this proximity becomes less important if (13) holds, as $\Gamma_{\mathcal{W}}$ nearly aligns with $\mathcal{N}_c$. This observation is investigated further in the next section.

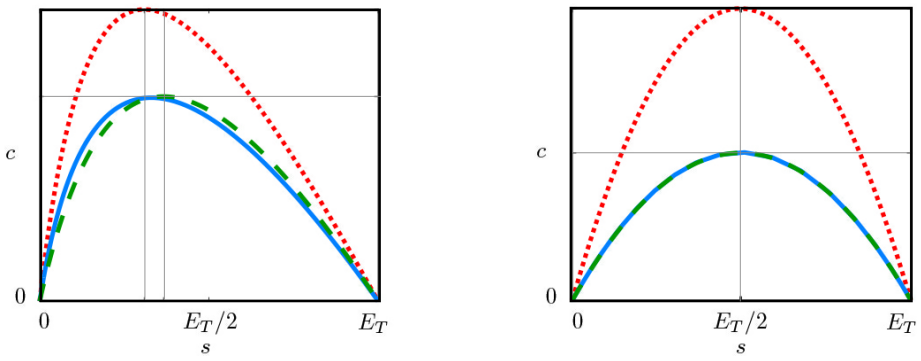


Figure 3: **The effect of condition** (13) **to the** $c$–$s$ **phase–plane geometry of the IAZA reaction mechanism** (3)**.** Each figure represents the rapid equilibrium nullcline $\mathcal{N}_s$ (dotted red line), quasi-steady-state nullcline $\mathcal{N}_c$ (stippled green line) and the heteroclinic orbit $\Gamma_{\mathcal{W}}$ (thick blue line). In both figures, the rate constants are $k_1 = k_{-1} = k_2 = 1$, so $K_M = 2$ with arbitrary units. On the figure to the left $E_T/K_M = 1$, but to the right, $E_T/K_M = 0.01$; thus, condition (13) is satisfied only in the latter case.

## 2.2 Steady-state kinetics: A preliminary comparison of the autocatalytic zymogen activation with the Michaelis–Menten reaction

In this section we will compare and contrast the steady-state kinetics of the MM and IAZA reactions mechanisms; these results are essential to understand the application of the popular model reduction technique of QSSA described in detail in the next section. Enzyme catalyzed reactions that evolve in QSS generally consist of two dynamical regimes: the initial *fast* transient phase and the *slow* QSS phase. During the transient phase the intermediate complex concentration, $c$, increases very rapidly while, in contrast, the depletion of substrate concentration, $s$, is negligible. Thus,

$$s \approx s_0 \tag{14}$$

during the transient phase. Formally, the approximation (14) is known as the reactant stationary assumption (RSA) [32, 3]. Immediately after the fast transient phase, the reaction is in the QSS phase, and $c$ changes very slowly. Therefore, it follows that

$$\frac{\mathrm{d}c}{\mathrm{d}t} \approx 0 \tag{15}$$

during the QSS phase of the reaction. Collectively, the characteristics (14) and (15) constitute the hallmark features of steady-state kinetics in the transient and QSS regimes, respectively.

Before we carry out a direct comparison between the QSS dynamics (i.e. the steady-state kinetics) of MM and IAZA reaction mechanisms, it will help to review the the necessary condition(s) that must hold in order for QSS dynamics to emerge, as well as some of the kinetic features that are unique to the MM reaction mechanism (2) when steady-state kinetics prevails. The mass action equations employed to model the MM reaction mechanism are:

$$\frac{\mathrm{d}s}{\mathrm{d}t} = -k_1 es + k_{-1} c, \tag{16a}$$

$$\frac{\mathrm{d}c}{\mathrm{d}t} = k_1 es - (k_{-1} + k_2) c, \tag{16b}$$

$$\frac{\mathrm{d}e}{\mathrm{d}t} = -k_1 es + (k_{-1} + k_2) c, \tag{16c}$$

$$\frac{\mathrm{d}p}{\mathrm{d}t} = k_2 c. \tag{16d}$$

It is well established [27, for more details], that if the initial enzyme concentration, $e_0$, is much less than $K_M + s_0$, then the MM reaction mechanism (2) will unfold in a QSS, and the MM equation (1) will hold for

the effective majority of the reaction. Formally, the condition

$$\varepsilon_{SS} \equiv \frac{e_0}{K_M + s_0} \ll 1 \tag{17}$$

is known as the RSA [32]. When (17) holds, the MM reaction mechanism (2) begins with a fast transient, during which the complex concentration accumulates rapidly to its maximum value. The rate of change of $c$ is identically zero once the complex concentration reaches its maximum value and intercepts the $c$-nullcline. The QSS phase of the reaction starts at the point of interception, and (15) as well as (1) simultaneously hold. Moreover, the *approximate* time it takes for $c$ to reach its peak value and for the reaction to reach the QSS phase is given by $t_C^*$:

$$t_C^* = \frac{|\ln \varepsilon_{SS}|}{k_1(K_M + s_0)}. \tag{18}$$

After the complex concentration reaches its threshold (maximum) value, it proceeds to decrease monotonically, and

$$\frac{\mathrm{d}c}{\mathrm{d}t} < 0 \tag{19}$$

for the duration of the reaction. Thus, the complex concentration increases monotonically for $t \lesssim t_C^*$, and decreases monotonically for $t_C^* \lesssim t$ (see FIGURE 4, as well as [33] for a mathematical justification of (18)). There is no qualitative change in the QSS kinetics of the MM reaction mechanism when $e_0 \leq s_0$ or $s_0 < e_0$

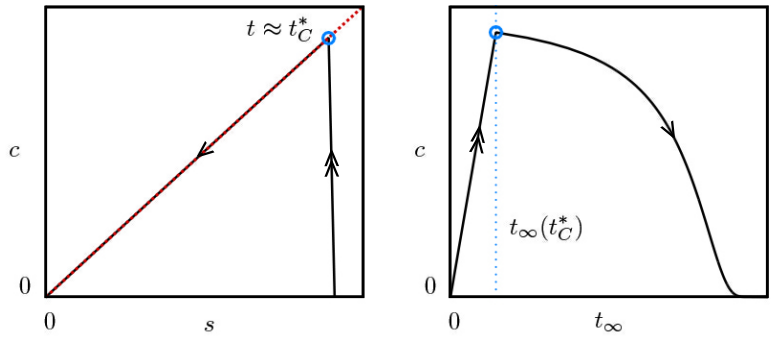


Figure 4: **The complex concentration, $c$, decreases monotonically during the QSS phase of the Michaelis–Menten reaction mechanism (2)**. The black curve is the numerical solution the mass action equations that model the MM reaction mechanism (2). "Double" arrows indicate *fast* dynamics; "single" arrows indicate *slow* dynamics. The time point $t = t_C^*$ is indicated by the blue open circle. In both panels, $k_1 = 0.1$, $k_2 = 100$, $k_{-1} = 100$, $e_0 = 1$ and $s_0 = 10$ in arbitrary units for illustrative purposes, thus $e_0 < s_0$. LEFT: This panel provides a graphical illustration of the QSS dynamics in the $c$–$s$ phase–plane. The trajectory (black curve) quickly approaches the $c$-nullcline (dotted red curve); the $c$-nullcline, along which $\mathrm{d}c/\mathrm{d}t = 0$, is given by $c = e_0 s/(K_M + s)$. Note that the approach to the $c$-nullcline is practically vertical, which corresponds to a negligible loss of substrate concentration. The trajectory reaches the $c$-nullcline at approximately $t_C^*$, at which point $c$ reaches its maximum value and the QSS phase of the reaction begins. During the QSS phase, the trajectory closely follows the $c$-nullcline, and $|\mathrm{d}c/\mathrm{d}t| \approx 0$ for the remainder of the reaction. RIGHT: This panel provides a graphical visualization of the time course corresponding to the LEFT PANEL, where $t_\infty$ is the infinity timescale: $t_\infty(t) = 1 - 1/\ln(t + \mathrm{e})$. During the transient phase $c$ accumulates rapidly until it reaches its maximum value, after which it begins to steadily decrease

as long as $\varepsilon_{SS} \ll 1$ (see, FIGURE 5). The QSS phase of the MM reaction mechanism corresponds to the slow depletion of *both* substrate and complex concentrations. Thus, the *slow* monotonic depletion of complex during the QSS phase, as well as the negligible loss of $s$ during the transient phase, are the hallmarks of the MM reaction mechanism when the RSA is valid.

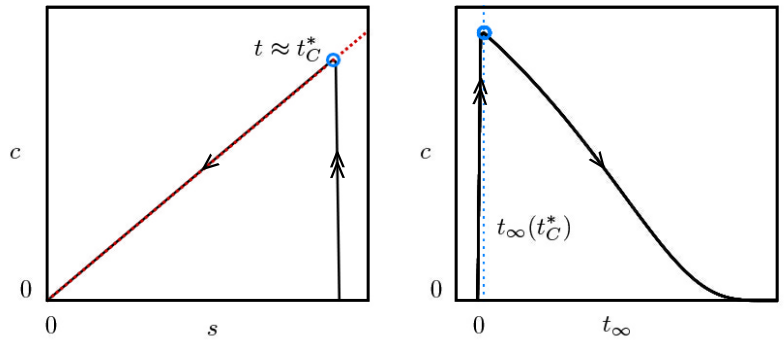


Figure 5: **The complex concentration, $c$, decreases monotonically during the QSS phase of the Michaelis–Menten reaction mechanism (2) when $s_0 < e_0$, provided $\varepsilon_{SS} \ll 1$.** In both panels, $k_1 = 0.1$, $k_2 = 100$, $k_{-1} = 100$, $e_0 = 10$ and $s_0 = 5$ in arbitrary units for illustrative purposes. Note that even though $s_0 < e_0$ the qualitative behavior is similar to the case when $e_0 < s_0$ (see FIGURE 4). Double arrows indicate fast dynamics; single arrows indicate slow dynamics. LEFT PANEL: In the phase–plane, $c$ increases rapidly while $s$ remains virtually constant. When $t \simeq t_C^*$, the trajectory intercepts the $c$-nullcline, and the QSS phase begins. RIGHT PANEL: $c$ decreases monotonically after the initial transient, and the qualitative dynamics are equivalent to the case when $e_0 < s_0$ in both the phase–plane and the time course. Thus, the ratio of $s_0$ and $e_0$ is not critical for the qualitative behavior of Michaelis–Menten reaction mechanism; the complex concentration decreases monotonically during the QSS phase as long as the RSA holds. In the time course, $t$ has been mapped to the $t_\infty$ timescale: $t_\infty(t) = 1 - 1/\ln(t + \mathrm{e})$.

We are now in a position to compare the qualitative dynamics of the IAZA reaction mechanism with the MM reaction mechanism. If QSS dynamics emerge when $\varepsilon \equiv E_T/K_M \ll 1$ holds for the IAZA reaction, then a rough estimate for the time it takes the reaction to reach the QSS phase is given by $t_C^\star$:

$$t_C^\star = \frac{|\ln \varepsilon|}{k_1(K_M + 2s_0)}. \tag{20}$$

We will justify (20) in Section (3.1) through scaling analysis and application of Tikhonov's Theorem. For the IAZA reaction mechanism, $t_C^\star$ delimits the transient and QSS phases of the reaction. During the transient phase, $s \approx s_0$, for $t \lesssim t_C^\star$; during the QSS phase the complex concentration changes vary slowly, and $\mathrm{d}c/\mathrm{d}t \approx 0$ for $t_C^\star \geq t$.

To compare the IAZA reaction mechanism with the MM reaction mechanism, we need to consider two cases: (1) $e_0 < s_0$ and, (2) $s_0 < e_0$. Let us start with case (1) illustrated graphically in FIGURE 6. If $e_0 < s_0$ and $\varepsilon \ll 1$, then there is a rapid initial increase of complex concentration until $t \simeq t_C^\star$, followed by the QSS phase, where the phase–plane trajectory closely follows the $c$-nullcline. Unlike the MM reaction mechanism (2), the complex concentration does not decrease monotonically during QSS phase: after $t \simeq t_C^\star$, $c$ continues to increase until $s \simeq E_T/2$ and the phase–plane trajectory intercepts the $c$-nullcline. After intercepting the $c$-nullcline, $c$ decreases monotonically for the remainder of the reaction. Case (2) corresponds to $e_0 < s_0$, and is illustrated graphically in FIGURE 7. If $s_0 < e_0$ but $\varepsilon \ll 1$, then we again observe an initial rapid increase in complex concentration. However, if $s_0 < e_0$, then the phase–plane trajectory intercepts the $c$-nullcline when $t \simeq t_C^\star$, and the complex concentration decreases monotonically during the QSS phase of the reaction. Thus, qualitatively, the QSS dynamics of the IAZA reaction mechamism is homologous to the QSS dynamics MM reaction mechanism when $s_0 \leq e_0$ and $\varepsilon \ll 1$.

# 3 Application of the quasi-steady-state approximation to autocatalytic zymogen activation

Different model reduction techniques can be applied to derive expressions to model and monitor the MM reaction mechanism [34]. The most widely used model reduction technique in enzyme kinetics is the QSSA.

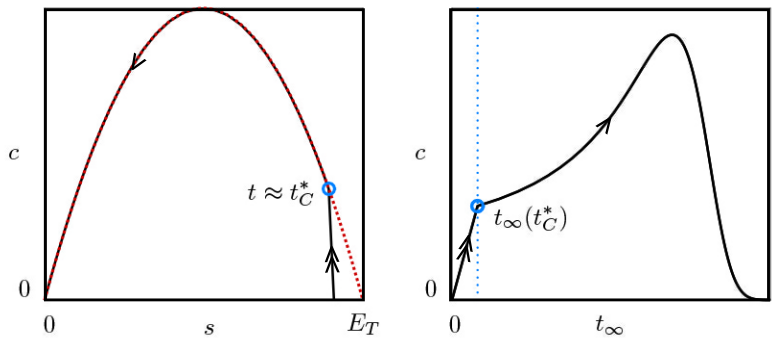


Figure 6: **The complex concentration, $c$, does not decrease monotonically during the QSS phase of the IAZA reaction mechanism (3) when** $e_0 < s_0$. LEFT: This panel provides a graphical illustration of the QSS dynamics in the $c$–$s$ phase–plane. The trajectory (black curve) quickly approaches the $c$-nullcline (dotted red curve) defined in Eq. (11) and reaches it at approximately $t_C^\star$. In contrast to the MM reaction mechanism (compare with FIGURES 4 and 5), the complex concentration continues to temporarily *increase* during the QSS phase of the reaction. The trajectory lies just underneath the $c$-nullcline while the complex concentration continues to accumulate; it crosses the $c$-nullcline when the complex reaches its maximum value and $s \approx E_T/2$, and then lies just above the $c$-nullcline for the remainder of the reaction. This behavior is in contrast to the QSS dynamics of the MM reaction mechanism, since $c$ decreases monotonically during the QSS phase when the RSA holds. The substrate concentration, $s$, is bounded between 0 and $E_T = s_0 + e_0$. RIGHT: This panel provides a graphical visualization of the time course corresponding to the LEFT PANEL. During the transient phase $c$ accumulates rapidly until it reaches the QSS phase when $t \simeq t_C^*$, and continues to steadily increase until it reaches its maximum value. $t$ has been mapped to the $t_\infty$ timescale: $t_\infty(t) = 1 - 1/\ln(t + \mathrm{e})$. In both panels, $k_1 = 0.1$, $k_2 = 100$, $k_{-1} = 100$, $e_0 = 1$ and $s_0 = 10$ in arbitrary units for illustrative purposes.

The effectiveness of this technique requires meeting certain restrictions for the initial conditions and rate constants of the reaction [27, 32]. In enzyme assays, the reaction achieves QSS when $c$ remains approximately constant over time, and the reaction rate changes relatively slowly. Rates are measured after reaching QSS by monitoring either the depletion of the substrate or the accumulation of product with time. Because the measurements are carried out after a very short period, the approximation $s \approx s_0$ can be made if there is an excess of substrate with respect to the enzyme in the reaction. From the mathematical point of view, under the QSSA, $s$ is the only variable that changes significantly over time, as $c$ remains in the QSS [35, 24, 26].

In the previous section, we found substantial differences in the nonlinear dynamics of the MM and IAZA reaction mechanisms. However, those differences do not affect the applicability of the QSSA to the IAZA reaction mechanism (3). The QSSA can be applied to the nonlinear dynamical system (8a)–(8b) of the IAZA reaction mechanism to obtain a single-variable equation for the zymogen depletion:

$$\frac{\mathrm{d}s}{\mathrm{d}t} \simeq -\frac{\mathrm{d}\hat{s}}{\mathrm{d}t} = \frac{k_2(E_T - \hat{s})\hat{s}}{K_M + \hat{s}}, \tag{21}$$

which is derived by replacing $c$ in (8a) with its QSS expression, $\hat{c}$:

$$c \simeq \hat{c} = \frac{(E_T - \hat{s})\hat{s}}{K_M + 2\hat{s}}. \tag{22}$$

Equation (21) is homologous to the MM equation (1). In the work that follows, we will denote $\hat{s}$ to be the solution to the zeroth-order approximation, and we will utilize "$s$" to denote the solution to the mass action model equations.

We hypothesize that the condition (13) is the validity criterion of the QSSA for the IAZA reaction mechanism (3). The premise for our hypothesis is shown in FIGURE 8. We find that $c$–$s$ phase–plane

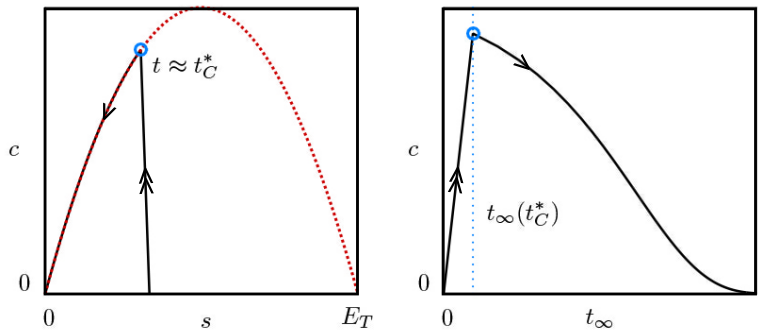


Figure 7: **The complex concentration, $c$, decreases monotonically during the QSS phase of the IAZA reaction mechanism (3) when $s_0 < e_0$.** Double arrows indicate fast dynamics; single arrows indicate slow dynamics. In both panels, $k_1 = 0.1$, $k_2 = 100$, $k_{-1} = 100$, $e_0 = 10$ and $s_0 = 5$ in arbitrary units for illustrative purposes. LEFT: This panel provides a graphical illustration of the QSS dynamics in the $c$–$s$ phase–plane. The trajectory (black curve) quickly approaches the $c$-nullcline (dotted red curve) defined in Eq. (11) and reaches it at approximately $t_C^\star$; it crosses the $c$-nullcline when the complex reaches its maximum value, and then lies just above the $c$-nullcline for the remainder of the reaction in a manner that is homologous to the MM reaction mechanism. Again, the almost vertical nature of the phase–plane trajectory during the transient phase is indicative of a minimal loss in substrate concentration. The substrate concentration, $s$, is bounded between 0 and $E_T = s_0 + e_0$. RIGHT: This panel provides a graphical visualization of the time course corresponding to the LEFT PANEL. During the transient phase $c$ accumulates rapidly until it reaches the QSS phase and its maximum value when $t \simeq t_C^*$. After the complex concentration reaches its maximum value it decreases monotonically for the remainder of the reaction. In the time course, $t$ has been mapped to the $t_\infty$ timescale: $t_\infty(t) = 1 - 1/\ln(t + \mathrm{e})$.

trajectories approach the $c$-nullcline vertically[1] and then closely follow the invariant manifold governing the steady-state kinetics in both the MM reaction mechanism (2) and IAZA reaction mechanism (3). In both cases, the invariant manifold is practically indistinguishable from the $c$-nullcline, because the condition (13) holds for the IAZA reaction mechanism, and the RSA holds for the MM reaction mechanism. In fact, for the MM reaction mechanism, the QSSA approximation is valid when the RSA holds [32]. We inspect the hypothetical validity of RSA for the IAZA reaction mechanism through scaling analysis [22] in the next section of this paper.

## 3.1 Scaling analysis of the governing equations for the autocatalytic zymogen activation

The QSSA is an important approximation that relies on the natural separation of timescales present in a chemical reaction. For a two-species system, the governing dynamical system consists of two timescales: a fast initial transient, and a slow QSS period [22, 24, 25]. In the case of the IAZA reaction mechanism, like the MM reaction mechanism [22], $s$ remains approximately constant while $c$ builds up rapidly during the initial fast transient. In the QSS phase, there is a measurable change in $s$, and the change in $c$ is dependent on the change in $s$. Formally, we say that $c$ is *slaved* by $s$ during the QSS phase of the reaction.

We now proceed to scale the nonlinear dynamical system (8a)–(8b) that governs the IAZA reaction mechanism (3). During the initial fast-transient (i.e., when $t \sim t_f$) $s$ remains approximately constant to its initial concentration ($s \approx s_0$). Therefore, we can approximate $\mathrm{d}s/\mathrm{d}t = 0$, which reduces (8a)-(8b) to a single differential equation for $c$:

$$\frac{\mathrm{d}c}{\mathrm{d}t} \simeq k_1 \Big[ s_0\, e_0 - (K_M + 2\, s_0)\, c \Big],$$

[1]Note we have not considered the applicability of a potential QSS reduction with respect to slow product formation and treated $k_2$ as a small parameter (i.e., in the limit as $k_2 \to 0$), in which case the nullclines coalesce, because this is not a catalytic case.

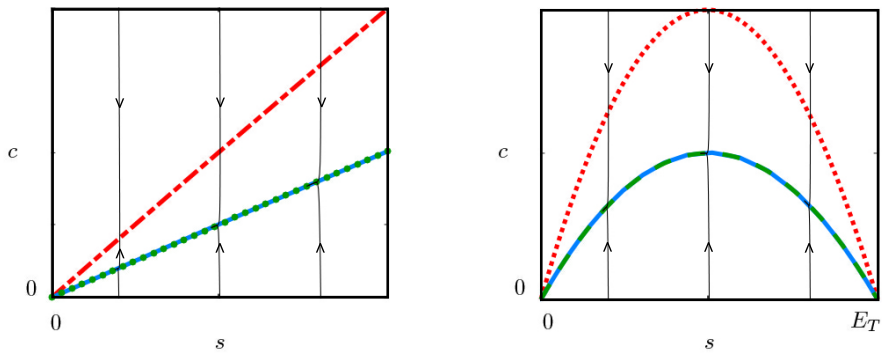


Figure 8: $c$–$s$ **phase–plane trajectories for the MM and IAZA reaction mechanisms when the conditions for the steady-state kinetics are valid.** The LEFT PANEL shows the $c$–$s$ phase–plane for the MM reaction mechanism (2) when the reactant-stationary approximation holds [32]. This approximation guarantees the validity of QSSA. The RIGHT PANEL shows the $c$–$s$ phase–plane for the IAZA reaction mechanism (3) when the condition (13) holds [32]. The substrate concentration, $s$, is bounded between 0 and $E_T = s_0 + e_0$ in the IAZA reaction mechanism. In both panels, the phase–plane trajectories approach and travel through $c$-nullcline which represent the invariant manifold governing the QSS dynamics of the reactions. The initial conditions for both panels are $(s_0, e_0) = \{(0.004, 0.016),\ (0.01, 0.01),\ (0.016, 0.004)\}$, thus $s_0 + e_0 = 0.02$ for each pair, implying $E_T = 0.02$ for the IAZA reaction mechanism. The Michaelis constant for both panels is $K_M = 2$. Initial conditions and parameters are expressed with arbitrary units for illustrative purposes.

with the initial condition $c(0) = 0$. The above differential equation can be solved analytically

$$c(t) \simeq \frac{s_0\, e_0}{K_M + 2s_0}\Big[1 - \exp\big(-k_1(K_M + 2\,s_0)\,t\big)\Big]. \tag{23}$$

From (23), we estimate the initial fast timescale $t_f$ to be

$$t_f = \frac{1}{k_1\big(K_M + 2\,s_0\big)}, \tag{24}$$

and define the scaled dimensionless time variable for the fast phase of the reaction as:

$$\tau = \frac{t}{t_f} = t\,k_1\big(K_M + 2\,s_0\big). \tag{25}$$

The matching concentrations between the initial fast transient and QSS period are $s(t_f) = s_0$ and $c(t_f) = (s_0\, e_0)/(K_M + 2\,s_0)$. These quantities allow us to define the following dimensionless variables:

$$\bar{s} = \frac{s}{s_0} \quad \text{and} \quad \bar{c} = \frac{K_M + 2\,s_0}{s_0\, e_0}\,c. \tag{26}$$

Substituting the scaled dimensionless variables (26) and timescale (25) into (8a)-(8b) yields the scaled nonlinear system governing the IAZA reaction mechanism during the initial fast timescale, $\tau$,

$$\frac{\mathrm{d}\bar{s}}{\mathrm{d}\tau} = \varepsilon\beta(1-\lambda)\bar{s}^2 + \varepsilon\lambda\beta^2(\alpha + 2\sigma\bar{s})\bar{c} - \varepsilon\beta\bar{s}, \tag{27a}$$

$$\lambda\frac{\mathrm{d}\bar{c}}{\mathrm{d}\tau} = \bar{s} - (1-\lambda)\bar{s}^2 - \lambda\beta(1 + 2\,\sigma\bar{s})\bar{c}. \tag{27b}$$

The dimensionless parameters that appear in (27a)–(27b) are:

$$\varepsilon \equiv \frac{E_T}{K_M},\ \ \lambda \equiv \frac{e_0}{e_0+s_0},\ \ \sigma = \frac{s_0}{K_M},\ \ k = \frac{k_{-1}}{k_2},\ \ \alpha \equiv \frac{k}{1+k} \text{ and } \beta \equiv \frac{1}{1+2\sigma}. \tag{28}$$

Although it appears (at first glance) that $\lambda$ may be a suitable small parameter the validity of the QSSA. However, note that $\lambda = 0$ is equivalent to $e_0 = 0$, from which we recover

$$\bar{s} = 0 \quad \text{or} \quad \bar{s} = 1. \tag{29}$$

Thus, $\lambda = 0$ implies that the initial condition lies on the fixed point located at $(s_0, 0)$ whenever $s_0$ is nontrivial and $e_0 = 0$. Consequently, $\varepsilon$ arises as a singular perturbation parameter that justifies the applicability of the QSSA via Tikhonov's Theorem. Defining $T = \tau/\varepsilon$ and using the scaled dimensionless variables (26) and parameters (28), we can scale the nonlinear system governing the IAZA reaction mechanism during the slow QSS phase to

$$\frac{\mathrm{d}\bar{s}}{\mathrm{d}T} = \beta(1-\lambda)\bar{s}^2 + \lambda\beta^2(\alpha + 2\sigma\bar{s})\bar{c} - \beta\bar{s}, \tag{30a}$$

$$\varepsilon\lambda\frac{\mathrm{d}\bar{c}}{\mathrm{d}T} = \bar{s} - (1-\lambda)\bar{s}^2 - \lambda\beta(1+2\,\sigma\bar{s})\bar{c}. \tag{30b}$$

Note that when $\varepsilon \ll 1$, $\mathrm{d}\tilde{c}/\mathrm{d}T$ is $\mathcal{O}(\varepsilon^{-1})$ while $\mathrm{d}\tilde{s}/\mathrm{d}T$ is $\mathcal{O}(1)$. These arguments confirm that the small singular parameter $\varepsilon = E_T/K_M \ll 1$ is a suitable condition for the validity of the QSSA, and delimits the governing nonlinear differential equations (8a)–(8b) for the IAZA reaction mechanism into a fast regime (27a)–(27b), and a slow regime (30a)–(30b). Moreover, if $\lambda$ is order unity, then the time it takes to reach the QSS phase of the reaction is

$$T \simeq \varepsilon|\ln\varepsilon|. \tag{31}$$

Since $T = \varepsilon t/t_f$, we recover $t_C^\star$ [see (20)] as the dimensional time it takes to reach the QSS phase of the reaction. The validity of the timescale $t_C^\star$ has already been verified numerically (see FIGURE 6), but rigorous arguments for the validity of analogous estimates can be found in [36] and [33].

## 3.2 Enzyme assays and the condition for the validity of the QSSA

In the laboratory, a wide variety of enzyme assays can be used to perform steady-state enzyme kinetics experiments, such as absorbance- and fluorescence-based assays. The equipment and materials for the enzyme assays will vary. Although enzyme assays provide limited information about the fundamental rate constants at the microscopic level, they are useful research tools that are commonly used to characterize enzyme or inhibitor activity, or compare the effects of mutations or modifications on enzymatic function.

The most commonly used type of experiment in enzyme kinetics measures the initial rate of an enzymatic reaction as a function of substrate concentration. Initial rate experiments are carried out under experimental conditions where the QSSA is valid. As we mentioned in Section 3, rates are measured after the initial fast-transient by monitoring the substrate depletion or accumulation of product over time. The initial rates measured are plotted versus substrate concentration. The kinetic parameters are determined by fitting the data to the MM equation using nonlinear regression if the mechanism of action follows the MM reaction mechanism (2) [6, 37, for more details]

For the IAZA reaction mechanism, the homologous rate law to the MM equation (21) for measuring the substrate depletion is:

$$\hat{v}_0 = -\frac{\mathrm{d}\hat{s}}{\mathrm{d}t} = \frac{k_2(E_T - \hat{s})\hat{s}}{K_M + 2\hat{s}}. \tag{32}$$

To determine the initial rate of autocatalytic zymogen activation using (32), the enzyme assay needs to meet the condition (13) for the validity of the QSSA; this is $\hat{s}_0 < E_T \ll K_M$. This condition requires $K_M$ for the IAZA reaction mechanism to be at least one order of magnitude larger than the reactants, $E_T$, in the enzyme assay. If no initial estimate for $K_M$ is available, a wide range of $E_T$ concentrations should be tried

and the range refined in subsequent enzyme assays as needed. Alternatively, $E_T$ can be more conveniently varied by adding or subtracting zymogen, rather than enzyme, at the start of the reaction.

The curve defined by (32) is shown in FIGURE 9. It has an unimodal shape that crosses the origin and $E_T$, and reaches a limiting rate of $\hat{v}$ at $\hat{s}_c^* \simeq E_T/2$ (the same concentration (12) that maximizes $\mathcal{N}_c(s)$ from (11)). Thus, when the condition (13) is valid, $\hat{s}_c^* = E_T/2$, $\hat{v}$ yields:

$$\hat{v} \approx \frac{1}{4}\frac{k_2 E_T^2}{K_M + E_T} \tag{33}$$

concentration The reaction is approximately zero order in $\hat{s}_c^*$ and is said to be saturated, because all of the active sites of the enzyme are occupied by a zymogen.

At very small values of $\hat{s}$, the denominator of the right-side (32) is dominated by $K_M$, so $\hat{s}$ is negligible compared to both $K_M$ and $E_T$, and $\hat{v}_0$ is directly proportional to $\hat{s}$ giving an initial slope approximately to

$$\hat{v}_0 \approx \frac{k_2 E_T}{K_M}\hat{s}. \tag{34}$$

This result implies that the reaction is approximately first-order overall at low $\hat{s}$, and $k_2 E_T/K_M$ is a first-order constant for the reaction. Similar to the MM reaction mechanism, $k_2 E_T/K_M$ is the specificity constant of the reaction, and $K_M/k_2 E_T$ is the specificity time. This is the time that would be required to consume all of the zymogen if the enzyme were acting under first-order conditions and maintained the same initial rate indefinitely [1].

For the MM reaction mechanism (2), $K_M$ is defined operationally as the substrate concentration that corresponds to one half of the limiting rate $v/2$. For (32), $K_M$ does not have the same operational definition. Under QSS conditions, when $\hat{v}/2$ in (32), $\hat{s}_{\hat{v}/2}$ has two values:

$$\hat{s}^-_{\hat{v}/2} \simeq \frac{E_T}{2}\left(1 - \frac{\sqrt{2}}{2}\right) \text{ and } \hat{s}^+_{\hat{v}/2} \simeq \frac{E_T}{2}\left(1 + \frac{\sqrt{2}}{2}\right). \tag{35}$$

The concentrations above are valid under (13), thus under the approximation $\hat{s}^* \simeq E_T/2$ from (12).

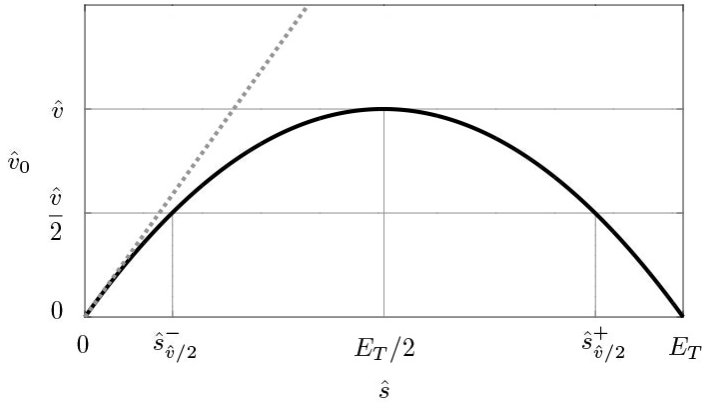


Figure 9: **The initial velocity of the IAZA mechanism under QSSA.** The initial velocity (32) is represented by the solid black line. The figure shows the limiting rate $\hat{v}$ defined by equation (33) and the operational concentrations $\hat{s}_{\hat{v}/2}$ defined as the values $\hat{s}$ when $\hat{v}/2$ (35). The initial slope $\hat{v}_0$ for $\hat{s} \approx 0$, defined by Eq. (34), is marked by the stippled grey line. Kinetic parameters and initial conditions are $k_2 = 1$, $E_T = 0.02$ and $K_M = 2$ with arbitrary units.

# 4 Estimation of the reaction completion time for the zymogen activation

The reaction completion time, $t_d$, is a timescale with practical applications in enzyme assays. It can be used to experimentally determine the molar enthalpy $\Delta H_{\text{app}}$ of an enzyme catalyzed reaction in calorimetry assays.

An enzyme rate can be determined by measuring the rate of heat generated upon substrate conversion into product, and estimate $K_M$ and $k_{\text{cat}}$ values. The magnitude of $\Delta H_{\text{app}}$ is estimated by allowing the reaction to proceed to completion and then integrating the calorimetry rate signal to obtain the total heat transferred. $\Delta H_{\text{app}}$ is proportional to $t_d$ [38].

For the IAZA reaction mechanism (3), the reaction reaches completion when the zymogen is depleted. Therefore, we formally represent, $t_d$, as:

$$t_d \approx \frac{\Delta s}{\max\left|\mathrm{d}\hat{s}/\mathrm{d}t\right|} = \frac{\text{Total change in } s \text{ after transient}}{\text{Maximum depletion rate of } s \text{ after transient}}. \tag{36}$$

Defining $\max|\mathrm{d}\hat{s}/\mathrm{d}t|$ in (36) to be the limiting rate of the zeroth-order approximation (21), we obtain:

$$\max\left|\frac{\mathrm{d}\hat{s}}{\mathrm{d}t}\right| = \begin{cases} \dfrac{k_2 E_T^2}{4(K_M + E_T)} & \text{for } e_0 \le s_0 \\ \dfrac{k_2\, e_0\, s_0}{K_M + 2\, s_0} & \text{for } s_0 < e_0 \end{cases}. \tag{37}$$

The dependency of $|\mathrm{d}\hat{s}/\mathrm{d}t|$ on the relation between $s_0$ and $e_0$ is critical – this is illustrated on FIGURE 10. The total change in $s$, $\Delta s$, is equal to the initial zymogen concentration $s_0$. Substituting $\Delta s = s_0$ and (37)

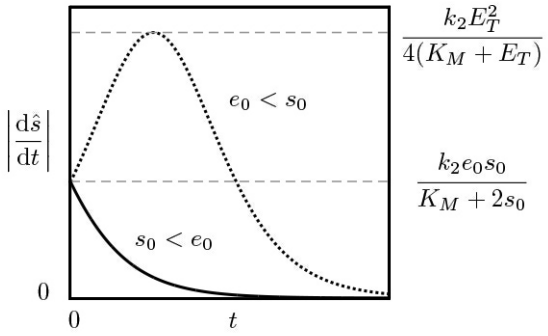


Figure 10: **Limiting rate of** (21) **changes with the relation between** $s_0$ **and** $e_0$. The figure shows the absolute velocity $|\mathrm{d}\hat{s}/\mathrm{d}t|$ for $s_0 = 0.00125 < e_0 = 0.00875$ (solid black) and for $e_0 = 0.00125 < s_0 = 0.00875$ (dotted black) and the corresponding maxima as defined in (37). Since for both cases $E_T = 0.01$ the initial velocities are equal, but it equals the maximal absolute velocity only for $s_0 < e_0$ ; when $e_0 > s_0$ the maximal velocity is achieved at $s \approx E_T/2$. In each situation, the QSSA is satisfied: $k_1 = k_2 = k_{-1} = 2$, thus the (13) is met. Initial conditions and parameter values are in arbitrary units for illustrative purposes.

into (36) yields an estimate for the completion time of the zymogen action

$$t_d = \frac{4s_0(K_M + E_T)}{k_2 E_T^2} \quad \text{for } e_0 \le s_0 \tag{38a}$$

$$t_d = \frac{K_M + 2s_0}{k_2 e_0} \qquad \text{for } s_0 \le e_0 \tag{38b}$$

Thus, the shape of the $c$-nullcline provides two choices for the depletion timescale. It is clear that both (38a) and (38b) are in exact agreement when $e_0 = s_0$. Further note that (38b) is homologous to the depletion timescale of the MM reaction mechanism (2) analyzed by Segel [27]. However, if $s_0 < e_0$, then (38a) may be too short to serve as a reasonable depletion timescale (see LEFT PANEL of FIGURE 11). In contrast, if $e_0 < s_0$, then (38b) provides a more conservative estimate of the depletion timescale in comparison to the more liberal estimate given by (38a) (see RIGHT PANEL of FIGURE 11). In either case, it is straightforward to show that $t_f/t_d \to 0$ as $\varepsilon \equiv E_T/K_M \to 0$. Thus, timescale separation is a consistent necessary (but not sufficient) condition for the validity of (21).

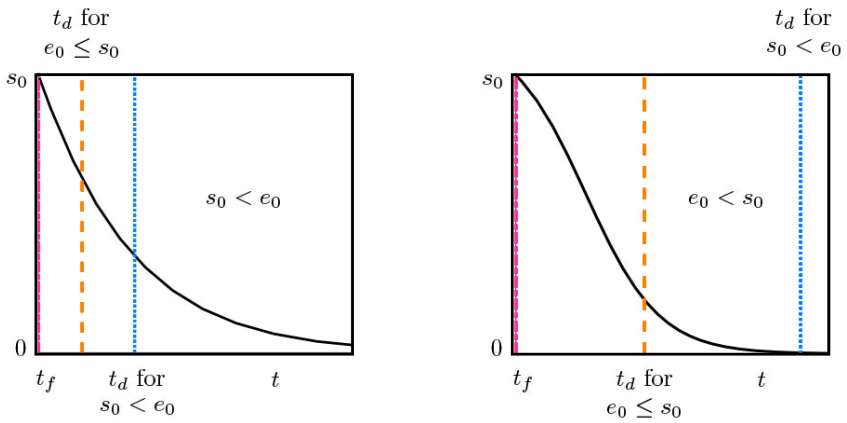


Figure 11: **Timescale for completion of the zymogen action as a function initial concentrations.** LEFT: Numerically computed progress curve for $s(t)$ (solid black) with the fast $t_f$ (dashed pink) timescale marked as vertical lines for reference. Because the initial conditions are $s_0 = 0.0125$, $e_0 = 0.0875$, the corresponding completion time scale is $t_d$ (38b) (marked by stippled blue line) must be chosen with respect to the condition $s_0 < e_0$. The dashed orange line shows the complementary estimate for $t_d$ from (38a); this time estimate is observed to be too short to characterize a completion of the reaction. The parameters used for the computation are $k_1 = k_2 = k_{-1} = 1$, thus $K_M = 2$ and $E_T = 1$. RIGHT: Same as to the left, but with $s(t)$ computed for $s_0 = 0.0875$, and $e_0 = 0.0125$. The estimate of the $t_d$ from (38a) (dashed orange line) approximates the completion time scale more liberally when chosen with respect to the condition $e_0 \leq s_0$, and the complementary estimate from (38b) (dashed orange) provides longer, more conservative estimate.

# 5 Discussion

The main contribution of this work is the analysis of a model for the autocatalytic zymogen activation (IAZA) reaction mechanism (3), and its comparison with the MM reaction mechanism (2). Although the mechanism of enzyme action is the same for both mechanisms, the nonlinear dynamics of both reaction mechanisms reveal distinct differences. We find that the nature of catalysis is a decisive factor in determining the specific dynamics and geometrical picture of the reaction.

One of the most fundamental dynamical differences between the IAZA and MM reaction mechanism is the number and stability of equilibria points. The MM reaction mechanism only exhibits one stable equilibrium, while the IAZA reaction mechanism exhibits an additional saddle equilibrium point. The existence of these two equilibria creates a heteroclinic orbit of unimodal shape between the saddle equilibrium and stable equilibrium points, which is the invariant manifold that influences the long-time dynamics of the IAZA reaction mechanism (3) in the $c$–$s$ phase–plane.

The critical result of this work is the derivation of an initial rate equation (21) – homologous to the MM equation – using the QSSA. This expression can be used to estimate the enzyme kinetics parameters by measuring the initial rates of the autocatalytic zymogen activation as a function of zymogen concentrations under the condition (13) for the validity of the QSSA. It should be pointed out that our analysis has been focused on the QSSA due to the fact that the QSSA is commonly utilized as a reduced model to determine kinetic parameters from initial rate experiments. However, there are other forms of the "QSSA" that are commonly implemented, such as the total QSSA, which was originally formulated by Laidler [39], or the reverse QSSA [40]. Subsequent analyses have improved our understanding of the conditions that lead to the validity of the total QSSA [41]. However, the tQSSA is typically utilized to estimate parameters from progress curve experiments, and introduces the experimental challenge of measuring the total substrate concentration. Hence, we have chosen not to analyze the conditions for the tQSSA in this work.

In addition, we also derived a mathematical expression to estimate the completion time of the zymogen activation, which can be used to experimentally determine the molar enthalpy $\Delta H_{\text{app}}$ of the autocatalytic zymogen reaction in calorimetry assays. It is possible that more general timescale estimates can be obtained

from the analysis of the total QSSA [42]. However, the timescale estimates derived in this work are sufficient for the region of parameter space that is our primary focus.

## Acknowledgement

Justin Eilertsen is supported by the University of Michigan Postdoctoral Pediatric Endocrinology and Diabetes Training Program "Developmental Origins of Metabolic Disorder" (NIH/NIDDK grant: K12 DK071212).

# References


[1] A. Cornish-Bowden, Fundamentals of enzyme kinetics, 4th Edition, Wiley-Blackwell, Weinheim, Germany, 2012.

[2] A. Cornish-Bowden, Current IUBMB recommendations on enzyme nomenclature and kinetics, Perspect. Sci. 1 (2014) 74–87.

[3] S. Schnell, Validity of the Michaelis–Menten equation – Steady-state or reactant stationary assumption: that is the question, FEBS J. 281 (2014) 464–472.

[4] W. Stroberg, S. Schnell, On the estimation errors of $K_M$ and $v$ from time-course experiments using the Michaelis—Menten equation, Biophys. Chem. 219 (2016) 17–27.

[5] D. L. Purich, Enzyme kinetics: Catalysis and Control, Elsevier, 2010.

[6] H. Bisswanger, Enzyme assays, Perspect. Sci. 1 (2014) 41–55.

[7] A. Cornish-Bowden, One hundred years of Michaelis–Menten kinetics, Perspect. Sci. 4 (2015) 3–9.

[8] J. Al-Janabi, J. A. Hartsuck, J. Tang, Kinetics and mechanism of pepsinogen activation, J. Biol. Chem. 247 (1972) 4628–4632.

[9] C. G. Sanny, J. A. Hartsuck, J. Tang, Conversion of pepsinogen to pepsin. Further evidence for intramolecular and pepsin-catalyzed activation, J. Biol. Chem. 250 (1975) 2635–2639.

[10] B. Kassell, J. Kay, Zymogens of proteolytic enzymes, Science 180 (1973) 1022–1027.

[11] A. R. Khan, M. N. G. James, Molecular mechanisms for the conversion of zymogens to active proteolytic enzymes, Protein Sci. 7 (1998) 815–836.

[12] E. C. Thrower, A. P. E. Diaz de Villalvilla, T. R. Kolodecik, F. S. Gorelick, Zymogen activation in a reconstituted pancreatic acinar cell system, Am. J. Physiol. Gastrointest. Liver Physiol. 290 (2006) G894–G902.

[13] J.-W. Wu, Y. Wu, Z.-X. Wang, Kinetic analysis of a simplified scheme of autocatalytic zymogen activation, Eur. J. Biochem. 268 (2001) 1547–1553.

[14] M. García-Moreno, B. H. Havsteen, R. Varón, H. Rix-Matzen, Evaluation of the kinetic parameters of the activation of trypsinogen by trypsin, Biochim. Biophys. Acta 1080 (1991) 143–147.

[15] M. E. Fuentes, R. Varón, M. García-Moreno, E. Valero, Kinetics of intra-and intermolecular zymogen activation with formation of an enzyme–zymogen complex, FEBS J. 272 (2005) 85–96.

[16] J. Eilertsen, W. Stroberg, S. Schnell, A theory of reactant-stationary kinetics for a mechanism of zymogen activation, Biophys. Chem. 242 (2018) 34–44.

[17] W.-N. Wang, X.-M. Pan, Z.-X. Wang, Kinetic analysis of zymogen autoactivation in the presence of a reversible inhibitor, Eur. J. Biochem. 271 (2004) 4638–4645.

[18] R. Varón, M. A. Minaya-Pacheco, F. García-Molina, E. Arribas, E. Arias, J. Masiá, F. García-Sevilla, Competitive and uncompetitive inhibitors simultaneously acting on an autocatalytic zymogen activation reaction, J. Enzyme Inhib. Med. Chem. 21 (2006) 635–645.

[19] M.-E. Fuentes, R. Varón, M. García-Moreno, E. Valero, Kinetics of autocatalytic zymogen activation measured by a coupled reaction: pepsinogen autoactivation, Biol. Chem. 386 (2005) 689–698.

[20] R. Varón, M. E. Fuentes, M. García-Moreno, F. García-Sevilla, E. Arias, E. Valero, E. Arribas, Contribution of the intra- and intermolecular routes in autocatalytic zymogen activation: Application to pepsinogen activation, Acta Biochim. Pol. 53 (2006) 407–420.

[21] F. G. Heineken, H. M. Tsuchiya, R. Aris, On the mathematical status of the pseudo-steady hypothesis of biochemical kinetics, Math. Biosci. 1 (1967) 95–113.

[22] L. A. Segel, M. Slemrod, The Quasi-Steady-State Assumption: A case study in perturbation, SIAM Rev. 31 (1989) 446–477.

[23] A. Goeke, C. Schilli, S. Walcher, E. Zerz, Computing quasi-steady state reductions, J. Math. Chem. 50 (2012) 1495–1513.

[24] L. Noethen, S. Walcher, Quasi-steady state and nearly invariant sets, SIAM J. Appl. Math 70 (2009) 1341–1363.

[25] A. Goeke, S. Walcher, E. Zerz, Classical quasi-steady state reduction – A mathematical characterization, Physica D 345 (2017) 11–26.

[26] A. Goeke, S. Walcher, Quasi-Steady State: Searching for and utilizing small parameters, in: Recent trends in dynamical systems, Vol. 35 of Springer Proc. Math. Stat., Springer, Basel, 2013, pp. 153–178.

[27] L. A. Segel, On the validity of the steady state assumption of enzyme kinetics, Bull. Math. Biol. 50 (1988) 579–593.

[28] A. H. Nguyen, S. J. Fraser, Geometrical picture of reaction in enzyme kinetics, J. Chem. Phys. 91 (1989) 186–193.

[29] S. Schnell, C. Mendoza, Closed form solution for time-dependent enzyme kinetics, J. Theor. Biol. 187 (1997) 207–212.

[30] A. Dhooge, W. Govaerts, Y. A. Kuznetsov, H. G. E. Meijer, B. Sautois, New features of the software MatCont for bifurcation analysis of dynamical systems, Math. Comput. Model. Dyn. Syst. 14 (2008) 147–175.

[31] A. Dhooge, W. Govaerts, Y. A. Kuznetsov, W. Mestrom, A. Riet, B. Sautois, MATCONT and CL MATCONT: Continuation toolboxes in MATLAB, Tech. rep., Universiteit Gent – Belgium and Utrecht University – The Netherlands (2006).

[32] S. M. Hanson, S. Schnell, Reactant stationary approximation in enzyme kinetics, J. Phys. Chem. A 112 (2008) 8654–8658.

[33] J. Eilertsen, W. Stroberg, S. Schnell, Characteristic, completion or matching timescales? an analysis of temporary boundaries in enzyme kinetics, J. Theor. Biol.

[34] S. Schnell, P. K. Maini, A century of enzyme kinetics. Reliability of the $K_M$ and $v_{\max}$ estimates, Comments Theor. Biol. 8 (2003) 169–187.

[35] M. R. Roussel, S. J. Fraser, Accurate steady-state approximations: Implications for kinetics experiments and mechanism, J. Phys. Chem. 95 (1991) 8762–8770.

[36] L. Noethen, S. Walcher, Quasi-steady state in the Michaelis-Menten system, Nonlinear Anal. Real World Appl. 8 (2007) 1512–1535. doi:10.1016/j.nonrwa.2006.08.004.
URL `https://doi.org/10.1016/j.nonrwa.2006.08.004`

[37] J. R. Lorsch, Practical steady-state enzyme kinetics, Methods Enzymol. 536 (2014) 3–15.

[38] M. J. Todd, J. Gomez, Enzyme kinetics determined using calorimetry: A general assay for enzyme activity?, Anal. Biochem. 296 (2001) 179–187.

[39] K. J. Laidler, Theory of the transient phase in kinetics, with special reference to enzyme systems, Can. J. Chem. 33 (1955) 1614–1624.

[40] S. Schnell, P. K. Maini, Enzyme kinetics at high enzyme concentration, Bull. Math. Biol. 62 (2000) 483–499.

[41] A. M. Bersani, E. Bersani, G. Dell'Acqua, M. G. Pedersen, New trends and perspectives in nonlinear intracellular dynamics: one century from Michaelis–Menten paper, Continuum Mech. Therm. 27 (2015) 659–684.

[42] J. A. M. Borghans, R. J. De Boer, L. A. Segel, Extending the quasi-steady state approximation by changing variables, Bull. Math. Biol. 58 (1996) 43–63.